A Numerical Study of Thermal Effects on Flow and Pollutant Dispersion in Urban Street Canyons

JAE-JIN KIM AND JONG-JIN BAIK

Department of Environmental Science and Engineering, Kwangju Institute of Science and Technology, Kwangju, Korea

(Manuscript received 17 August 1998, in final form 30 October 1998)

ABSTRACT

This study investigates thermal effects on the flow and pollutant dispersion in urban street canyons. A two-dimensional numerical model with a k–ϵ turbulent closure scheme is developed, and the heat transfer between the air and the building wall or street-canyon bottom is effectively represented by a wall function. For each of seven cases with different aspect ratios (building height/width between buildings = 0.5, 1, 1.5, 2, 2.5, 3, and 3.5), four thermal situations (no heating, upwind building-wall heating, street-canyon bottom heating, and downwind building-wall heating) are considered.

In the cases of upwind building-wall heating, one vortex appears regardless of aspect ratio. When the aspect ratio is greater than or equal to 1.5, the upward motion forced by upwind building-wall heating overcomes the downward motion that appears in the cases of no heating. In the cases of street-canyon bottom heating, when the aspect ratio is less than 3, flow patterns are similar to those in the cases of upwind building-wall heating. This similarity is because the maximum temperature axis is shifted toward the upwind side by the horizontal motion. However, when the aspect ratio is 3 or 3.5, the horizontal velocity is not strong enough to shift the maximum temperature axis toward the upwind side. When the maximum temperature axis is located near the center of the street canyon, two counterrotating vortices appear side by side in the lower layer due to the thermal upward motion around the axis, while the vortex in the upper layer is little influenced by bottom heating. With downwind building-wall heating, two counterrotating vortices appear except in the 0.5 aspect ratio case. To a large extent, the vortex in the upper layer is mechanically induced by the ambient wind, while the vortex in the lower layer is thermally induced by downwind building-wall heating.

The dispersion of pollutants released at the street level is shown to be quite dependent upon aspect ratio and heat source location. The vortex number and intensity greatly influence the residue concentration ratio (ratio of the total pollutant amount remaining in the street canyon to the total amount of pollutants emitted) by controlling the travel pathway and escape time of pollutants.

1. Introduction

The urban canopy is composed of basic elements such as isolated or in-group buildings and street canyons. The main factors that determine the flow field in urban street canyons include both geometrical and meteorological factors. The geometrical factors include the building shape and orientation and the aspect ratio, which is defined as a ratio of the building height to the width between buildings. The aspect ratio is an important factor that determines flow regimes in urban street canyons. These regimes can be categorized into isolated roughness flow, wake interference flow, and skimming flow (Oke 1988; Hunter et al. 1992; Sini et al. 1996). In the skimming flow regime, which appears in relatively deep street canyons, the transition from a one- to a two-vortex regime and from a two- to a three-vortex regime occurs as the aspect ratio increases. When counterrotating vortices are present, the escape time of pollutants from the street canyon to the ambient air is delayed not only because the pollutant transport from the lower layer to the upper layer in the street canyon is dominated by the diffusion process (Lee and Park 1994) but also because the travel pathway is elongated.

The meteorological factors that influence street-canyon flow include incident wind speed and direction, atmospheric stability, solar irradiation, and so on. From a field experiment in a street canyon with an aspect ratio of about 1.5, DePaul and Sheih (1986) suggested that the threshold ambient wind speed necessary to generate one vortex is about 1.2 m s^{-1}. Hoydysh and Dabberdt (1988) examined the effects of varying the incident wind direction to street canyons on the concentration distribution of pollutants in the wind tunnel. In general, the distribution patterns are divided into the cross-street regime and the along-street regime according to the in-

Corresponding author address: Prof. Jong-Jin Baik, Dept. of Environmental Science and Engineering, Kwangju Institute of Science and Technology, 572 Sangamdong, Kwangsan-ku, Kwangju 506-712, Korea.
E-mail: jjbaik@aromi.kjist.ac.kr

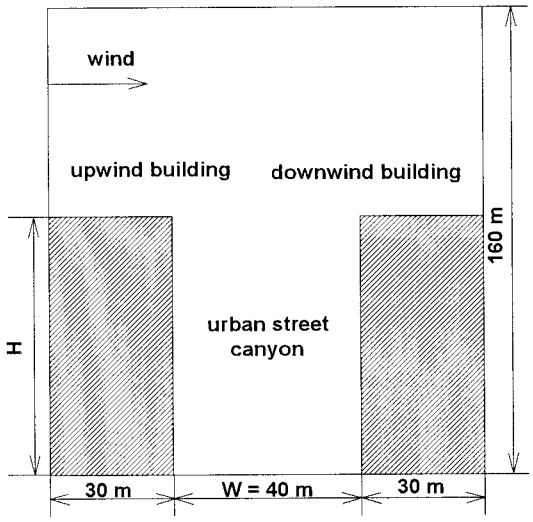

FIG. 1. The model domain configuration for this study.

cident angle of the ambient wind. Their results measured at the upwind and downwind sides do not agree with the assumption (Johnson et al. 1971) that the concentration distribution pattern does not change in each regime. Baik and Kim (1999), using a two-dimensional numerical model with a k–ϵ turbulent closure scheme, examined the effect of wind speed on the counterrotating vortices in a street canyon with an aspect ratio of 2. They showed that the threshold ambient wind speed near the roof level required to generate two counterrotating vortices is 3.7 m s^{-1}.

The parameters that determine solar heating in street canyons are the orientation, wall property, albedo, and emissivity of building; the sky view factor; and so on (Nunez and Oke 1977; Sakakibara 1996). Nakamura and Oke (1988) measured temperatures in a street canyon with an aspect ratio of 1.06 and a sky view factor of 0.43. They found that the maximum temperature difference between the air and the building surfaces in the street canyon approaches values as large as 12°–14°C. This large temperature difference is because the building and street are composed mainly of concrete and asphalt, which have low heat capacity. Using an energy balance model that takes into account the sky view factor, Sakakibara (1996) showed that the urban thermal environment depends on urban geometry through reduced sky view factors and complicated daytime shadow patterns. Sini et al. (1996) numerically investigated the effect of wall heat flux by solar heating in the street canyon. They pointed out the importance of thermal effects on the

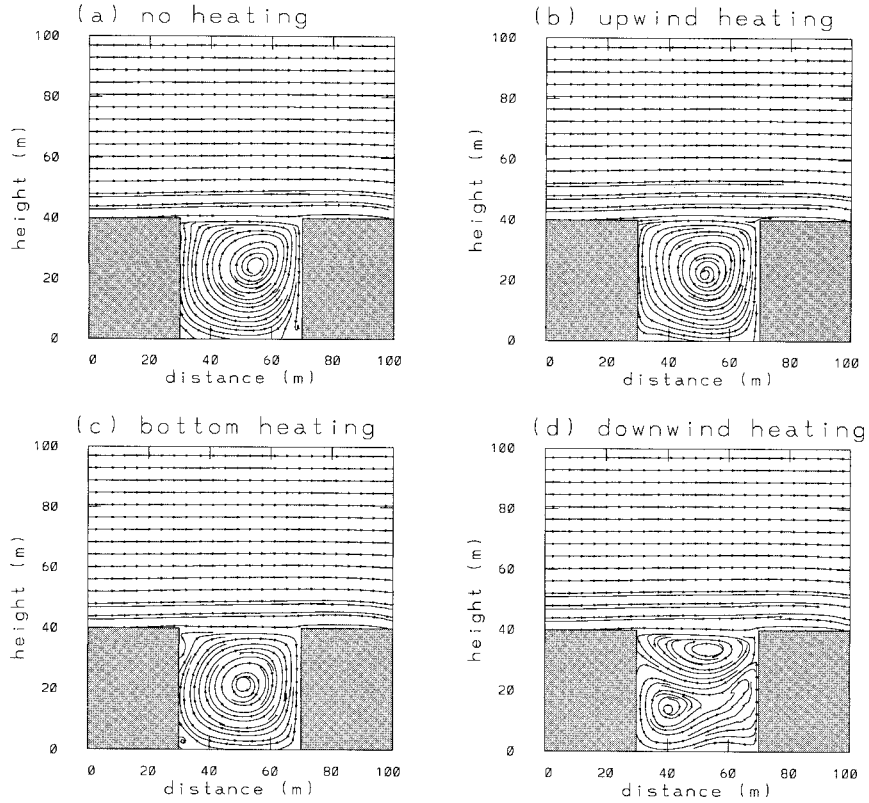

FIG. 2. Streamline fields at $t = 1$ h for an aspect ratio of 1 in the cases of (a) no heating, (b) upwind building-wall heating, (c) street-canyon bottom heating, and (d) downwind building-wall heating.

flow and pollutant dispersion. However, in their study the aspect ratio was restricted to 1.12.

In this study, the thermal effects on the flow and pollutant dispersion in urban street canyons with a wide range of aspect ratios will be examined systematically. For this purpose, a two-dimensional numerical model with a k–ϵ turbulent closure scheme is developed, and the heat transfer between the air and the building wall or street-canyon bottom is represented by a wall function.

2. Description of numerical model

The numerical model used in this study is the same as that of Baik and Kim (1999) except that the thermodynamic energy equation is included to simulate thermal effects. In a two-dimensional (x–z plane), nonhydrostatic, nonrotating, and Boussinesq airflow system, the momentum equations in the horizontal and vertical directions, the mass continuity equation, the thermodynamic energy equation, and the transport equation for pollutant concentration can be written as

$$\frac{\partial U}{\partial t} + U\frac{\partial U}{\partial x} + W\frac{\partial U}{\partial z} = -\frac{1}{\rho}\frac{\partial P}{\partial x} + \frac{\partial}{\partial x}\left(K_m\frac{\partial U}{\partial x}\right) + \frac{\partial}{\partial z}\left(K_m\frac{\partial U}{\partial z}\right), \quad (1)$$

$$\frac{\partial W}{\partial t} + U\frac{\partial W}{\partial x} + W\frac{\partial W}{\partial z} = -\frac{1}{\rho}\frac{\partial P}{\partial z} + g\frac{\Theta - \Theta_n}{\Theta_n} + \frac{\partial}{\partial x}\left(K_m\frac{\partial W}{\partial x}\right) + \frac{\partial}{\partial z}\left(K_m\frac{\partial W}{\partial z}\right), \quad (2)$$

$$\frac{\partial U}{\partial x} + \frac{\partial W}{\partial z} = 0, \quad (3)$$

$$\frac{\partial \Theta}{\partial t} + U\frac{\partial \Theta}{\partial x} + W\frac{\partial \Theta}{\partial z} = \frac{\partial}{\partial x}\left(K_\Theta\frac{\partial \Theta}{\partial x}\right) + \frac{\partial}{\partial z}\left(K_\Theta\frac{\partial \Theta}{\partial z}\right) + S_\Theta, \quad (4)$$

and

$$\frac{\partial C}{\partial t} + U\frac{\partial C}{\partial x} + W\frac{\partial C}{\partial z} = \frac{\partial}{\partial x}\left(K_C\frac{\partial C}{\partial x}\right) + \frac{\partial}{\partial z}\left(K_C\frac{\partial C}{\partial z}\right) + S_C. \quad (5)$$

Here, t is the time, U the mean (gridpoint) velocity in the x direction, W the mean velocity in the z direction, Θ the mean potential temperature, C the mean pollutant concentration, ρ the air density, P the mean pressure deviation, g the gravitational acceleration, and Θ_n the potential temperature at the reference state. The terms K_m, K_Θ, and K_C are the turbulent diffusivities for momentum, heat, and pollutant concentration, respectively. Note that K_m (or K_Θ, K_C) is the same in all directions. In (4) S_Θ denotes the heat source term, and in (5) S_C denotes the source term of pollutants.

The turbulent diffusivities are determined from the turbulent kinetic energy (k) and its dissipation (ϵ). The prognostic equations for these variables can be written in our flow system as

$$\frac{\partial k}{\partial t} + U\frac{\partial k}{\partial x} + W\frac{\partial k}{\partial z} = K_m\left\{2\left[\left(\frac{\partial U}{\partial x}\right)^2 + \left(\frac{\partial W}{\partial z}\right)^2\right] + \left(\frac{\partial U}{\partial z} + \frac{\partial W}{\partial x}\right)^2\right\} - K_\Theta\frac{g}{\Theta_n}\frac{\partial \Theta}{\partial z} + \frac{\partial}{\partial x}\left(\frac{K_m}{\sigma_k}\frac{\partial k}{\partial x}\right) + \frac{\partial}{\partial z}\left(\frac{K_m}{\sigma_k}\frac{\partial k}{\partial z}\right) - \epsilon, \quad (6)$$

$$\frac{\partial \epsilon}{\partial t} + U\frac{\partial \epsilon}{\partial x} + W\frac{\partial \epsilon}{\partial z} = C_{\epsilon 1}\frac{\epsilon}{k}K_m\left\{2\left[\left(\frac{\partial U}{\partial x}\right)^2 + \left(\frac{\partial W}{\partial z}\right)^2\right] + \left(\frac{\partial U}{\partial z} + \frac{\partial W}{\partial x}\right)^2\right\} - C_{\epsilon 1}K_\Theta\frac{\epsilon}{k}\frac{g}{\Theta_n}\frac{\partial \Theta}{\partial z} + \frac{\partial}{\partial x}\left(\frac{K_m}{\sigma_\epsilon}\frac{\partial \epsilon}{\partial x}\right) + \frac{\partial}{\partial z}\left(\frac{K_m}{\sigma_\epsilon}\frac{\partial \epsilon}{\partial z}\right) - C_{\epsilon 2}\frac{\epsilon^2}{k}, \quad (7)$$

where

$$K_m = C_\mu\frac{k^2}{\epsilon}, \quad (8)$$

$$\mathrm{Pr}_t = \frac{K_m}{K_\Theta}, \quad \text{and} \quad (9)$$

$$\mathrm{Sc}_t = \frac{K_m}{K_C}. \quad (10)$$

The terms on the right-hand side of (6) and (7) represent the shear production term, the buoyancy production term, the turbulent diffusion terms in the x and z directions, and the dissipation term, respectively. The nondimensional parameters Pr_t and Sc_t in (9) and (10) are the turbulent Prandtl number and the turbulent Schmidt number, respectively. The constants used in (6)–(10) are specified as (Sini et al. 1996)

$$(C_\mu, \sigma_k, \sigma_\epsilon, C_{\epsilon 1}, C_{\epsilon 2}, \mathrm{Pr}_t, \mathrm{Sc}_t) = (0.09, 1.0, 1.3, 1.44, 1.92, 0.7, 0.9). \quad (11)$$

The above governing equation set is solved numerically on a staggered grid system using the finite-volume method (finite area in two dimensions) following the Semi-Implicit Method for Pressure-Linked Equation (SIMPLE) algorithm described by Patankar (1980). In this algorithm, at each time step the tentative horizontal and vertical velocities are first obtained under an assumed pressure field. Then, the pressure change needed to adjust the velocity field so as to satisfy the mass

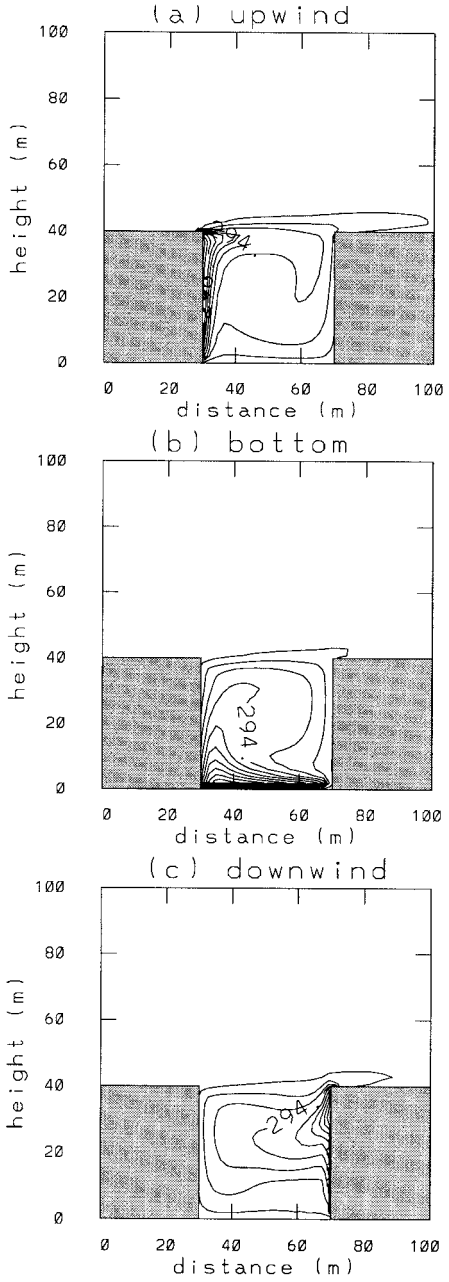

FIG. 3. Potential temperature fields (in K) at $t = 1$ h for an aspect ratio of 1 in the cases of (a) upwind building-wall heating, (b) street-canyon bottom heating, and (c) downwind building-wall heating. The contour interval is 0.5 K.

continuity is calculated by solving a pressure–Poisson equation. The final velocity and pressure fields are computed using the velocity and pressure correction equations, respectively.

Based upon the works by Abadie and Schiestel (1986) and Ciofalo and Collins (1989), the wall function is derived to represent effectively the heat transfer between the air and the building wall or street-canyon bottom:

$$\frac{Q_w}{\rho C_p} = \frac{U_*^2}{U_f}\frac{(\Theta_f - \Theta_w)}{\mathrm{Pr}_t(1 + \phi/s)}, \tag{12}$$

$$\phi = 9.24\left[\left(\frac{\mathrm{Pr}}{\mathrm{Pr}_t}\right)^{3/4} - 1\right] \times \left[1 + 0.28\exp\left(-0.007\frac{\mathrm{Pr}}{\mathrm{Pr}_t}\right)\right], \tag{13}$$

and

$$s = \frac{1}{\kappa}\ln\left(\frac{z_f}{z_0}\right). \tag{14}$$

Here, U_* is the friction velocity, ϕ the Jayatilleke function (Jayatilleke 1969), C_p the specific heat at constant pressure, Pr the Prandtl number, and κ the von Kármán constant ($=0.4$). The subscripts w and f denote the wall and the nearest grid point from the wall, respectively. The roughness length z_0 is specified as 5 cm (Sini et al. 1996).

In this study, a main concern is to examine thermal effects on the flow and concentration distribution in urban street canyons. For this, seven different aspect ratios are considered and for each aspect ratio there are no heating (hereinafter, denoted by NH), upwind building-wall heating (UH), street-canyon bottom heating (BH), and downwind building-wall heating (DH) cases. The horizontal and vertical domain sizes are 100 m and 160 m, respectively, and the grid interval is 2 m in both directions. The time step is 0.2 s. The width between the upwind and downwind buildings is fixed at 40 m but the building height varies. The aspect ratios considered are 0.5, 1, 1.5, 2, 2.5, 3, and 3.5. Figure 1 shows the model domain configuration for this study. The initial conditions for wind velocities, turbulent kinetic energy and its dissipation, and air potential temperature are specified as follows:

$$U_0 = 2.5\left(\frac{z}{z_r}\right)^{0.299}, \tag{15}$$

$$W_0 = 0, \tag{16}$$

$$k_0 = 0.003U_0^2, \tag{17}$$

$$\epsilon_0 = \frac{C_\mu^{3/4}k_0^{3/2}}{\kappa z}, \quad \text{and} \tag{18}$$

$$\Theta_{a0} = 293\ \text{K}. \tag{19}$$

Here, the reference height z_r is 10 m. Initially, the shear layer given by (15) is assumed to exist up to $z = 10$ m above the building roof level and above it the velocity is assumed to be constant. The building-wall or street-canyon bottom potential temperature is maintained at 298 K until the end of the numerical integration.

At the ground and building surfaces, the no-slip boundary condition is applied. The flow remains un-

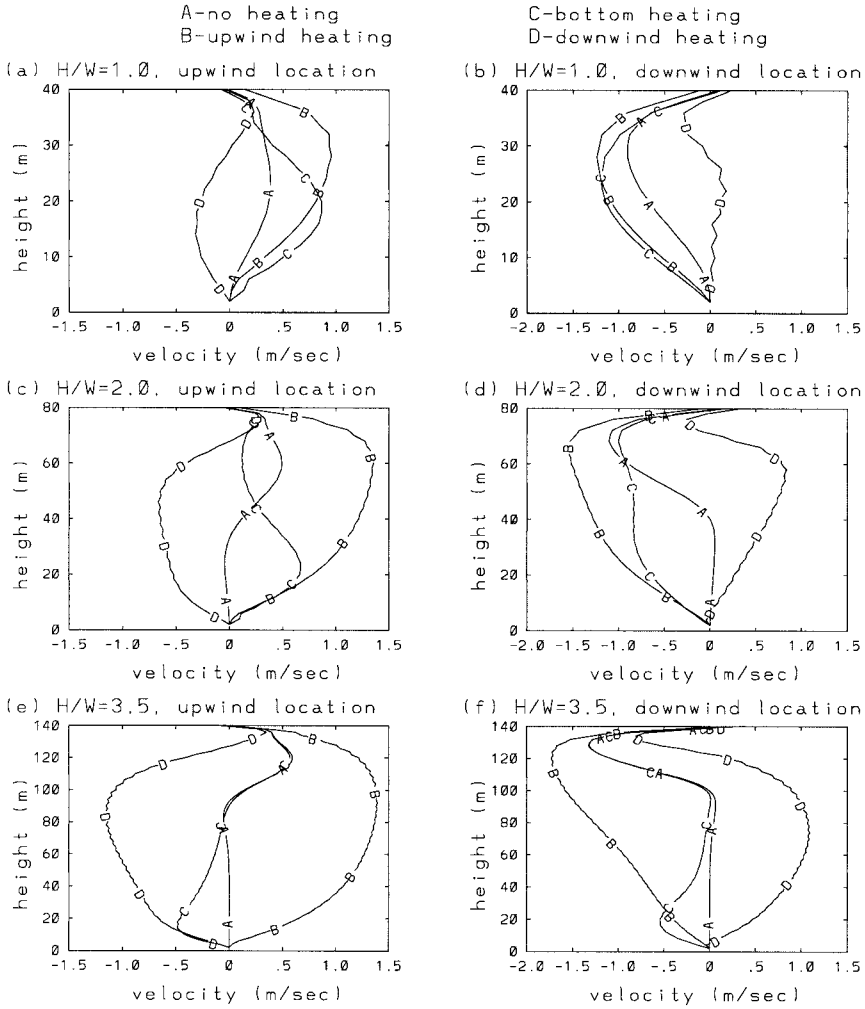

FIG. 4. The vertical profiles of vertical velocity at $x = 34$ m (near the upwind building) and $x = 66$ m (near the downwind building) in street canyons with aspect ratios of 1 [(a) and (b)], 2 [(c) and (d)], and 3.5 [(e) and (f)]. Note different vertical axis scales on the individual figures.

changed with time at the inflow boundary, while the gradient of any variable is set to zero at other boundaries.

3. Results and discussion

a. Flow characteristics

In order to examine simulated flow fields in urban street canyons when thermal effects are neglected (no-heating cases) and to compare these results with those obtained with thermal effects included, seven no-heating cases with different aspect ratios were analyzed first. Results showed that, similar to previous studies (e.g., Lee and Park 1994), as the aspect ratio increases, the transition from a one- to a two-vortex regime and from a two- to a three-vortex regime occurs. In the current model, one vortex appears for aspect ratios of 0.5 and 1; two vortices appear for aspect ratios of 1.5, 2, 2.5, and 3; and three vortices appear for aspect ratio of 3.5. It is not clear whether the case with an aspect ratio of 0.5 belongs to the wake interference flow regime or the skimming flow regime. However, according to the flow identification by Hunter et al. (1990–91), this case appears to be closer to the wake interference flow regime than to the skimming flow regime. The other six cases belong to the skimming flow regime.

A wind tunnel study by Hoydysh and Dabberdt (1988) showed one vortex in a canyon with an aspect ratio of 1.2. A similar numerical experiment with an aspect ratio of 1.2 was performed (NH case) and the result showed one vortex. This result is consistent with that of Hoydysh and Dabberdt (1988).

Figure 2 shows the streamline fields at $t = 1$ h in an urban street canyon with an aspect ratio of 1 in the cases of no heating, upwind building-wall heating, street-canyon bottom heating, and downwind building-wall heating. In the NH case, one vortex appears. In the UH or

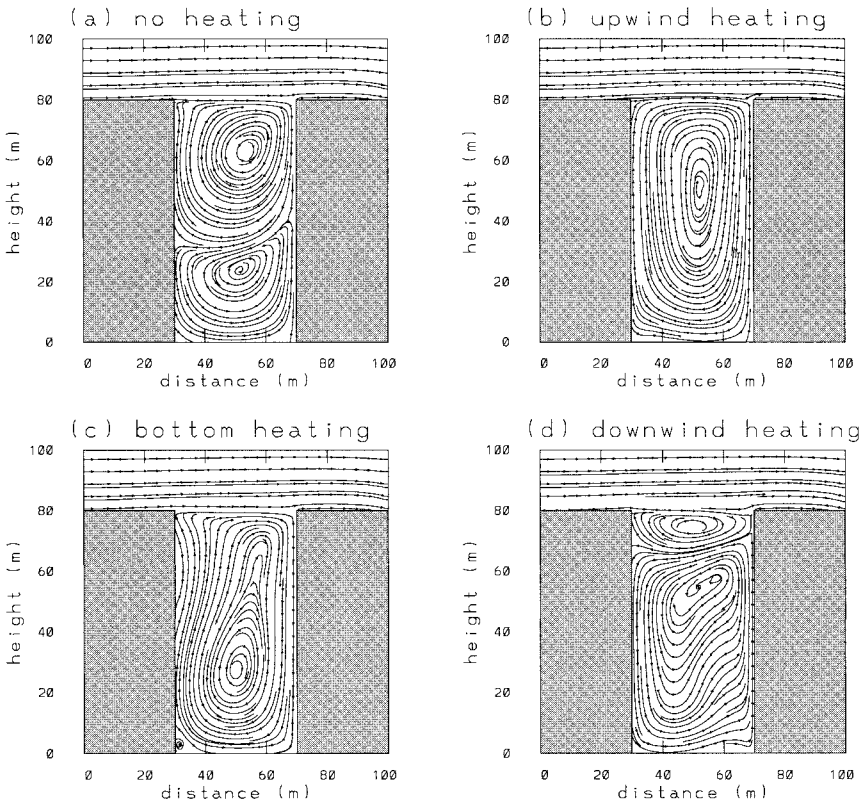

FIG. 5. The same as in Fig. 2 except for an aspect ratio of 2.

BH cases, one vortex appears as well. On the other hand, in the DH case, two counterrotating vortices appear. This result is consistent with the numerical modeling result of Sini et al. (1996).

The potential temperature field corresponding to the UH case (Fig. 3a) shows that the horizontal temperature gradient is large near the upwind building. Relatively warm air is advected downwind in the upper layer of the canyon in accordance with the vortex circulation. The higher potential temperature near the upwind building (positive buoyancy) induces upward motion on the upwind side. This thermal upward motion strengthens the vortex by enhancing the upward motion (Fig. 2a) that is mechanically induced by the ambient wind. The strengthened vortex in comparison with the NH case can be seen clearly in the vertical profiles of vertical velocity at the upwind and downwind locations (Figs. 4a and 4b).

In the BH case, the vertical potential temperature gradient near the street-canyon bottom and the horizontal potential temperature gradient near the upwind building are large (Fig. 3b). If there is no wind within a street canyon, the vertical axis of the maximum potential temperature would be located at the center of the street canyon. However, due to the horizontal motion toward the upwind building in the lower layer, the axis is shifted to the location close to the upwind building in the lower layer. In the upper layer, the axis is tilted downwind. Along this axis, thermally induced upward motion exists. This thermal upward motion near the upwind building strengthens the vortex by enhancing the upward motion (Fig. 2a) that is mechanically induced by the ambient wind. Figure 4a shows that, at the upwind location, the maximum vertical velocity in the BH case is observed near the midlevel of the street canyon, while the maximum vertical velocity in the UH case is observed above the midlevel.

In the potential temperature field corresponding to the DH case (Fig. 3c), the horizontal potential temperature gradient is large near the downwind building in the upper layer of the street canyon. There appears to be positive temperature advection toward the upwind building near the midlevel. At $z \sim 28$ m near the downwind building, the thermal upward motion cancels out the mechanical downward motion (Fig. 2d) [the vertical velocity becomes zero at this level (Fig. 4b)] and horizontal motion toward the upwind building occurs. This motion makes two counterrotating vortices (Fig. 2d). As can be seen in the vertical profiles of vertical velocity, the vortex weakens considerably at the downwind location because of the opposing mechanical and thermal effects on the vertical velocity near the downwind building (Fig. 4b).

Figure 5 shows the streamline fields in a street canyon with an aspect ratio of 2. For this aspect ratio, two counterrotating vortices form when there is no heating

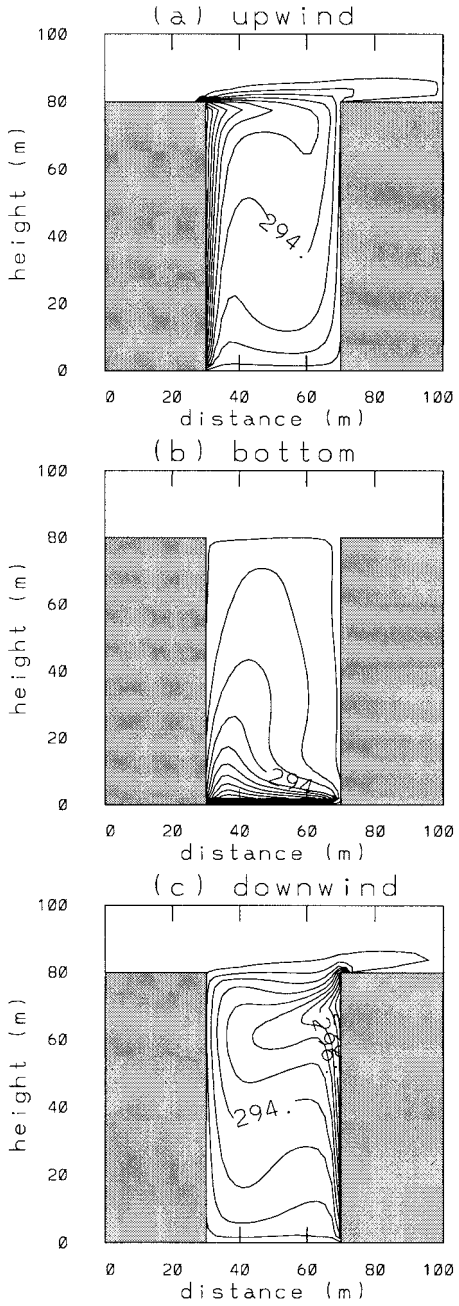

FIG. 6. The same as in Fig. 3 except for an aspect ratio of 2.

(Fig. 5a). These two counterrotating vortices are mechanically induced. When there is upwind building-wall heating (Fig. 5b) or street-canyon bottom heating (Fig. 5c), only one vortex forms by the combination of the two counterrotating vortices that appear in the NH case. When there is downwind building-wall heating (Fig. 5d), two counterrotating vortices appear as in the NH case. However, compared with the NH case, the intensity and vertical extent of the lower vortex increase and those of the upper vortex decrease due to the thermal upward motion near the downwind building (Figs. 4c and 4d).

The patterns of the potential temperature field for an aspect ratio of 2 (Fig. 6) are similar to those for an aspect ratio of 1 (Fig. 3). In the UH case (Fig. 6a), the thermal upward motion near the upwind building weakens due to the mechanical downward motion in the lower layer but strengthens due to the mechanical upward motion in the upper layer. As a result, one vortex is generated in the street canyon. In the BH case (Fig. 6b), the vertical axis of the maximum potential temperature is shifted to the upwind side. This results in one vortex by inducing upward motion near the upwind building. In the DH case with an aspect ratio of 2 (Fig. 6c), an increase of the temperature gradient in the middle and lower layers near the downwind building compared with that in the DH case with an aspect ratio of 1 (Fig. 3c) further intensifies thermally induced upward motion in the lower layer and weakens mechanically induced downward motion in the upper layer.

Figure 7 shows the streamline fields in a street canyon with an aspect ratio of 3.5. In the NH case, three mechanically induced counterrotating vortices appear. In the UH case, one vortex appears as in the cases for aspect ratios of 1 and 2 (Figs. 2b and 5b), and the strong horizontal potential temperature gradient (Fig. 8a) induces strong upward motion near the upwind building. This thermal upward motion causes the mechanical downward motion to disappear in the middle layer and causes the mechanical upward motion of the clockwise rotating vortices in the lower and upper layers to strengthen. The driving force for the thermal upward motion seen in this study is positive buoyancy due to the wall or bottom heating. As the building height increases, the region of strong driving force becomes deeper and the vortex becomes strengthened. This effect can be seen in the vertical profiles of vertical velocity in Fig. 4.

In the BH case (Fig. 7c), three vortices appear: two counterrotating vortices in the lower layer and one vortex in the upper layer. The potential temperature field (Fig. 8b) exhibits a symmetric pattern about the center of the street canyon. This is because the horizontal motion of the clockwise-rotating vortex is not strong enough to shift the maximum potential temperature axis to the upwind side and thus weakening or eliminating the counterclockwise-rotating vortex on the upwind side of the lower layer. In addition, the flow field in the upper layer is little influenced by the street-canyon bottom heating (see Figs. 4e, 4f, 7a, and 7c).

In the DH case, the patterns of the streamline field (Fig. 7d) with two counterrotating vortices and the potential temperature field (Fig. 8c) are similar to those in the cases for aspect ratios of 1 and 2. The intensity of the lower vortex increases with increasing building height because an increase in the heated wall height causes thermal upward motion to become stronger (see Figs. 4b, 4d, and 4f). Note that in the cases of downwind building-wall heating two counterrotating vortices appear except for the case with an aspect ratio of 0.5.

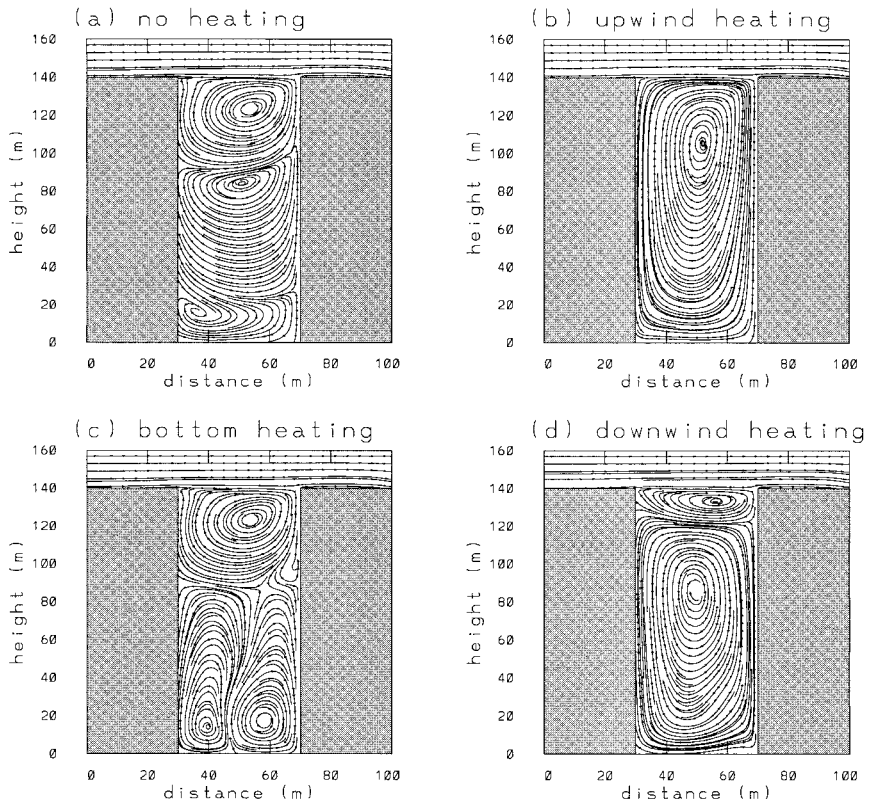

FIG. 7. The same as in Fig. 2 except for an aspect ratio of 3.5. Note different vertical axis scale from that in Figs. 2 and 5.

The effects of building-wall or street-canyon bottom heating in street canyons on the flow field can be drawn schematically as in Fig. 9. In the UH cases (Figs. 9a and 9b), a large horizontal temperature gradient near the upwind building causes upward motion there. When the aspect ratio is small, the thermal and mechanical upward motion make the vortex intensity stronger. When the aspect ratio is relatively large, two counterrotating vortices generated in the NH case are combined by the process in which the thermal upward motion enhances the mechanical upward motion of the upper clockwise-rotating vortex but dissipates the mechanical downward motion of the lower counterclockwise-rotating vortex (Fig. 9b). In the BH case with a small aspect ratio (Fig. 9c), the flow pattern is similar to that in the corresponding UH case (Fig. 9a) because the maximum temperature axis is shifted to the upwind side by the horizontal motion of the vortex. For a relatively large aspect ratio where two or three counterrotating vortices appear, two lower vortices first appear due to the strong thermal upward motion around the maximum temperature axis. Of the two vortices, the clockwise-rotating vortex is combined with the upper vortex. If the horizontal motion of the combined vortex is strong enough to shift the maximum temperature axis to the upwind side, the counterclockwise-rotating vortex disappears, and the resultant flow pattern is similar to that in the UH case (Fig. 9c). Otherwise, the two counterrotating vortices exist compatibly with the maximum temperature axis located near the center of the street canyon (Fig. 9d). When the aspect ratio is relatively small in the DH case (Fig. 9e), the thermal upward motion near the downwind building is weak compared with the mechanical downward motion and thereby a clockwise-rotating vortex appears. However, when the aspect ratio is relatively large (Fig. 9f), the mechanical downward motion and thermal upward motion balance at some height and two counterrotating vortices appear. As the aspect ratio increases, the lower vortex becomes relatively stronger.

Figure 10 shows the turbulent kinetic energy fields on a log contour scale when the aspect ratio is 1. In the NH case, the turbulent kinetic energy is high near the top of the upwind and downwind buildings and on the downwind side of the upper street canyon. The budget analysis of turbulent kinetic energy showed that near the downwind building of the upper canyon, the turbulent kinetic energy is high not only because of its vigorous production by the strong wind shear but also because of the advection of high turbulent kinetic energy from the roof level. The budget analysis in the UH and BH cases showed that the wind shear and advection are dominant factors in an increase of turbulent kinetic energy near the downwind building in the upper layer. In

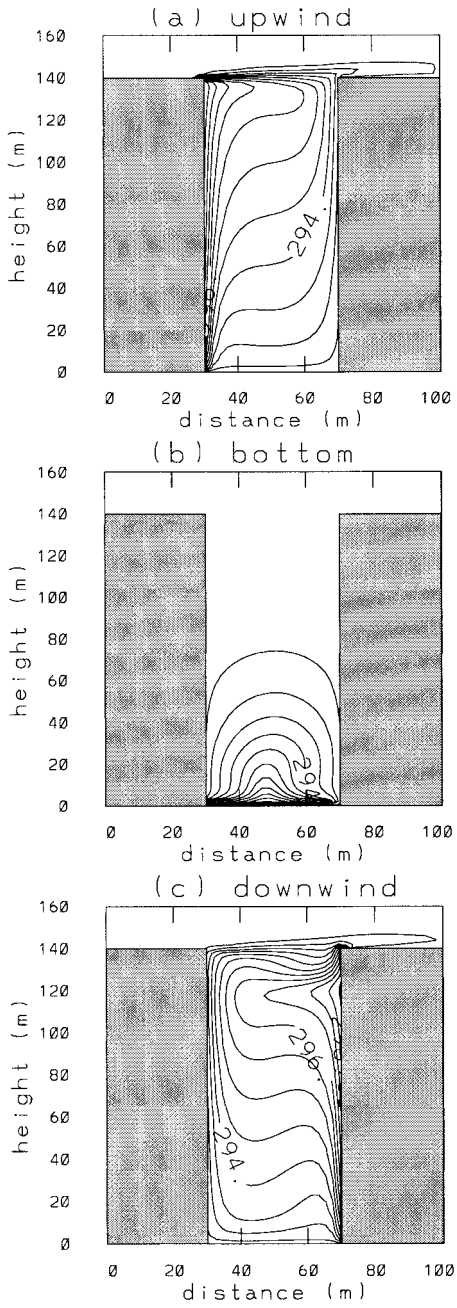

FIG. 8. The same as in Fig. 3 except for an aspect ratio of 3.5. Note different vertical axis scale from that in Figs. 3 and 6.

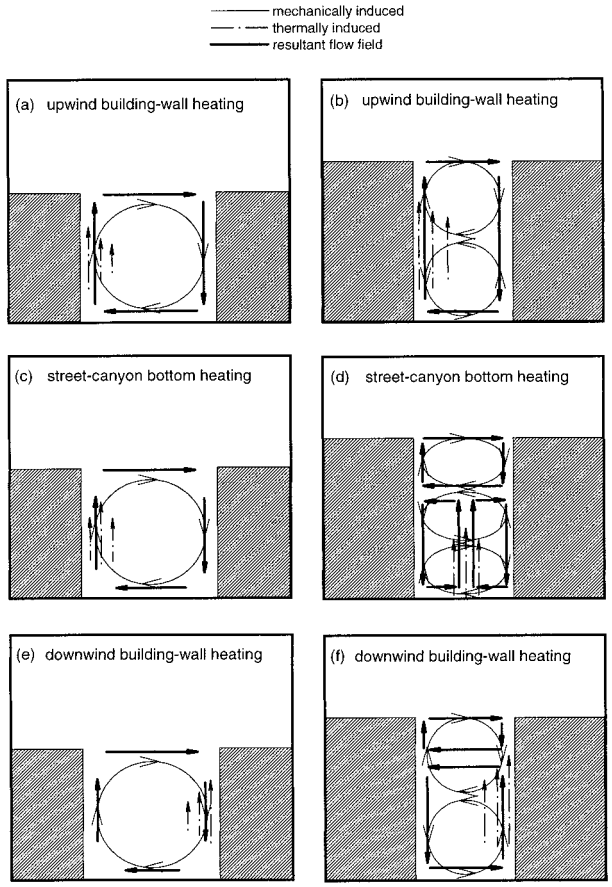

FIG. 9. The schematic diagrams for the flow patterns resulting from upwind building-wall heating [(a) and (b)], street-canyon bottom heating [(c) and (d)], and downwind building-wall heating [(e) and (f)] in street canyons with different aspect ratios (left and right). The resultant flow fields are drawn in rectangular shapes just for the clarity of the figures.

the UH case, there is suppression of turbulent kinetic energy by the buoyancy term in the region of ~38 m $< x <$ ~60 m in the middle and upper canyon because of the positive vertical potential temperature gradient. On the other hand, in the BH case, there is production of turbulent kinetic energy by the buoyancy term because of the negative vertical potential temperature gradient as a result of street-canyon bottom heating. In the DH case, the turbulent kinetic energy is relatively high near the downwind building in the upper layer due to its production by the wind shear and buoyancy. Since the vertical potential temperature gradient is positive on the downwind side below $z = 28$ m, there is suppression of turbulent kinetic energy by the buoyancy term. This suppression results in low turbulent kinetic energy.

b. Pollutant dispersion characteristics

In section 3a, we investigated thermal effects on the flow fields in urban street canyons with different aspect ratios for the cases of upwind building-wall heating, street-canyon bottom heating, and downwind building-wall heating. In this section, the dispersion characteristics of pollutants are investigated when there is continuous emission from the street level for the given flow fields. Using the flow fields at $t = 1$ h, the conservation equation of pollutants is integrated numerically until $t = 2$ h. Pollutants are emitted continuously from the street-level source having 20 emission points at a rate of 5 ppb s^{-1}. The pollutants released are assumed to be dispersing passively. In this study, results are compared

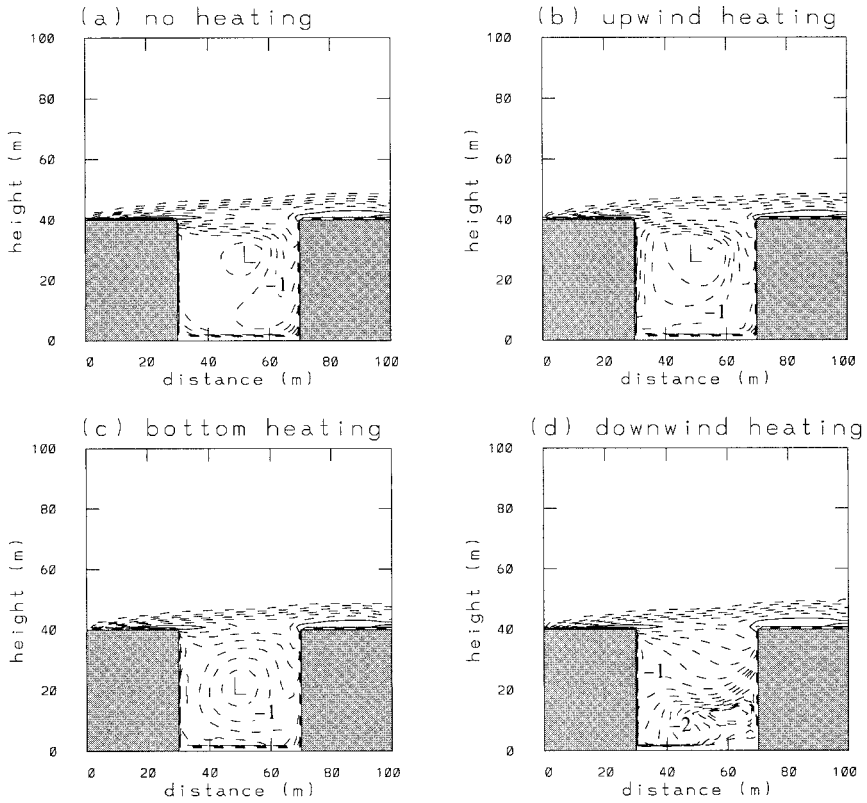

FIG. 10. Turbulent kinetic energy fields ($m^2 s^{-2}$) at $t = 1$ h for an aspect ratio of 1 in the cases of (a) no heating, (b) upwind building-wall heating, (c) street-canyon bottom heating, and (d) downwind building-wall heating. The values are on a log scale in base 10. The contour interval is 0.2.

using the residue concentration ratio, which is defined as the ratio of the total amount of pollutants remaining in the street canyon to the total amount of pollutants emitted during the integration.

Figure 11 shows the residue concentration ratio as a function of the aspect ratio. In the NH case, the residue concentration ratio increases up to an aspect ratio of 2 and then remains almost constant with aspect ratio. This

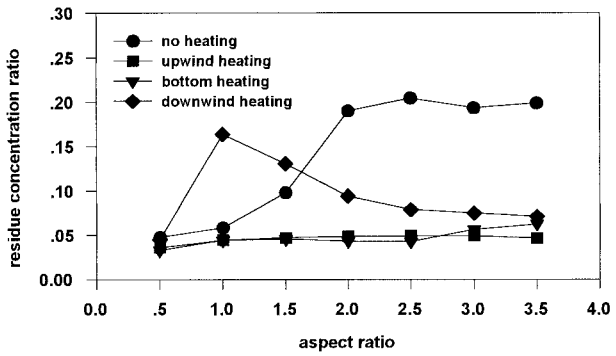

FIG. 11. The residue concentration ratio at $t = 2$ h as a function of the aspect ratio in the cases of no heating, upwind building-wall heating, street-canyon bottom heating, and downwind building-wall heating.

is related to the number and intensity of vortices produced in the street canyon. The travel pathway of pollutants in the two-vortex regime (aspect ratio = 1.5, 2, 2.5, 3) is elongated compared with that in the one-vortex regime (aspect ratio = 0.5, 1). In addition, the escape time from the street level to the ambient air is delayed because the intensity of the lower vortex is very weak and the pollutant transport between two counterrotating vortices is dominated by the diffusion process. Although the travel pathway associated with the one vortex produced in the UH case becomes longer, the residue concentration ratio is nearly constant because the vortex strengthening compensates for the longer pathway. The residue concentration ratio in the BH case is almost the same as that in the UH case. In the DH case, the residue concentration ratio is largest when the aspect ratio is 1 because of the presence of two counterrotating vortices. As the aspect ratio increases, the corresponding vortex intensity increases, hence the residue concentration ratio decreases.

Figure 12 shows the pollutant concentration fields on a log contour scale for an aspect ratio of 1. The pattern of the concentration distribution in the UH or BH cases is similar to that in the NH case. This is because in these three cases one vortex appears and the concentration

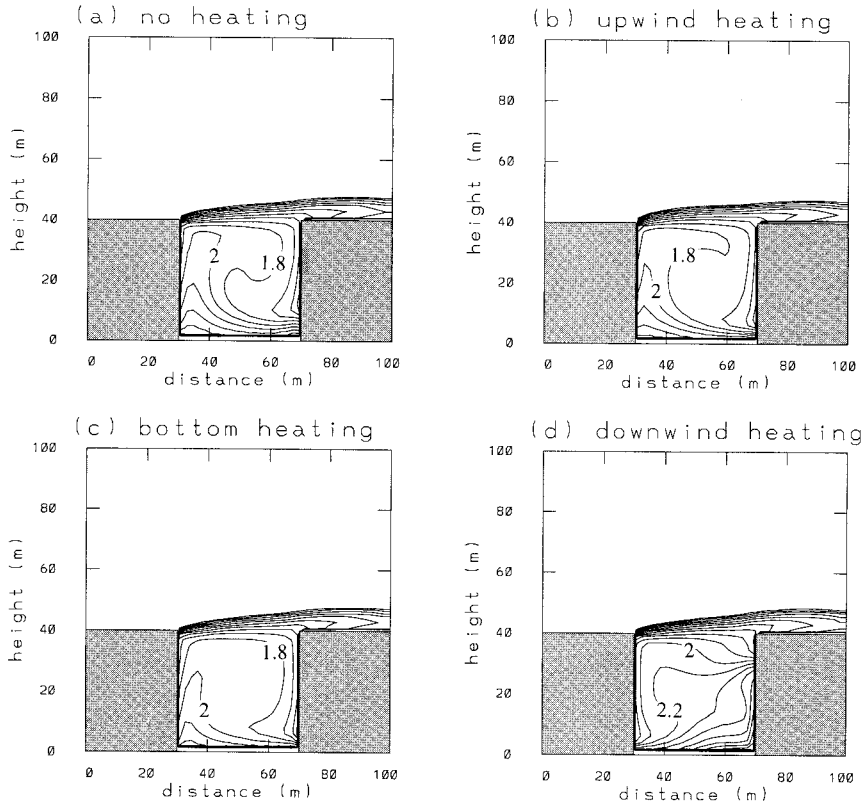

FIG. 12. Concentration distribution fields at $t = 2$ h for an aspect ratio of 1 in the cases of (a) no heating, (b) upwind building-wall heating, (c) street-canyon bottom heating, and (d) downwind building-wall heating. The values are on a log scale in base 10. The contour interval is 0.2.

distribution is controlled mainly by the vortex circulation. In the NH, UH, and BH cases, near the downwind building where the air having relatively low concentration comes into the street canyon, the concentration is lowest at any height, while near the upwind building where the air that passed through the emission source goes to the upper layer as a result of the advection and diffusion processes, the concentration is highest at any height. Some portion of pollutants transported to the upper layer escapes from the street canyon along the roof level and another portion goes down into the street canyon. The concentration budget analysis along the roof level showed that vertical diffusion is the chief contributor to the escape of pollutants from the street canyon. The concentration distribution pattern in the NH case is similar to that in a numerical study by Lanzani and Tamponi (1995). In the DH case where two counterrotating vortices appear, some portion of the pollutants transported to the middle height of the street canyon is transported to the upper vortex, mainly by the diffusion process, and some escapes from the street canyon after being transported to the roof level. In the UH and BH cases, in which the vortex is strengthened by the thermal upward motion, as the travel time of pollutants is shortened, the average concentration and residue concentration ratio in the street canyon decrease by 24% compared with those in the NH case (Fig. 11). However, in the DH case in which the travel pathway is elongated by the presence of two counterrotating vortices, the average concentration and residue concentration ratio increase by 180% compared with those in the NH case (Fig. 11).

Figure 13 shows the pollutant concentration fields for an aspect ratio of 2. Each pattern of the concentration distribution in the UH, BH, and DH cases, respectively, is similar to that corresponding to an aspect ratio of 1. The transport mechanism of pollutants is also similar. In the NH case with two counterrotating vortices, the intensity of the lower vortex is very weak. In the DH case, which also has two counterrotating vortices, the momentum transferred from the upper vortex and the buoyancy caused by the wall heating maintain the lower vortex at a stronger intensity (Figs. 4e and 4f) and therefore the escape time is shorter than in the NH case. The residue concentration ratios in the UH, BH, and DH cases decrease by 74%, 77%, and 51%, respectively, compared with that in the NH case (Fig. 11). As shown in Figs. 11, 12, and 13, the building-wall or street-canyon bottom heating has a significant influence on the concentration distribution by controlling the travel pathway and escape time of pollutants.

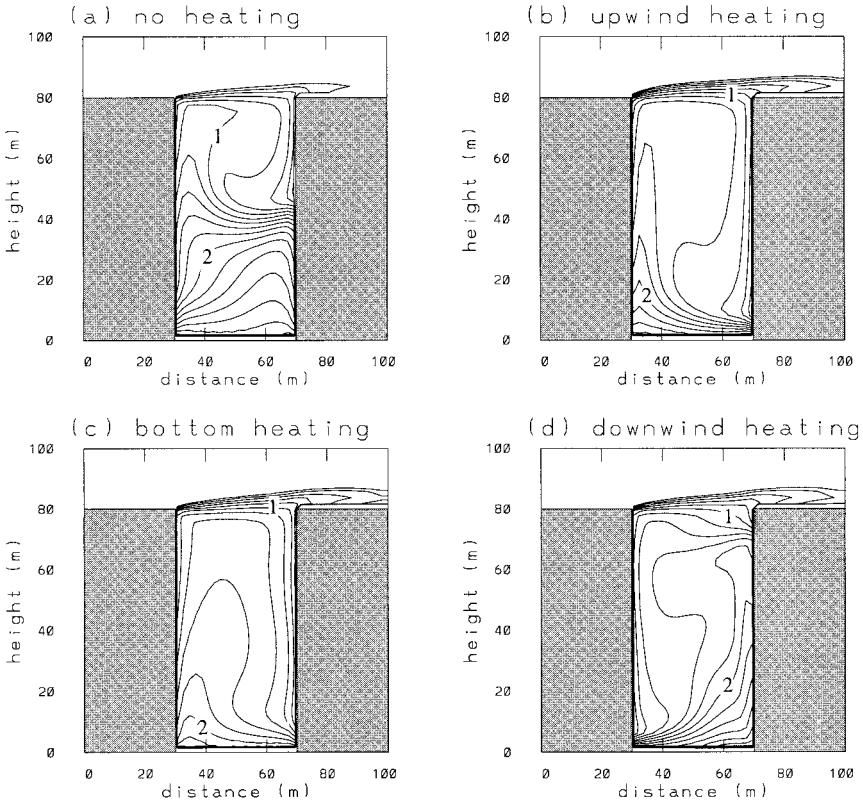

FIG. 13. The same as in Fig. 12 except for an aspect ratio of 2.

4. Summary and conclusions

Field, wind tunnel, and numerical studies on flow and dispersion in the street canyon have been carried out for the past two decades, but few studies on thermal effects have been performed. In this study, thermal effects on the flow and pollutant dispersion in urban street canyons were investigated systematically using a two-dimensional numerical model with a k–ϵ turbulent closure scheme. The heat transfer between the air and the building wall or street-canyon bottom was represented by a wall function. Numerical simulations were performed with four thermal situations (no heating, upwind building-wall heating, street-canyon bottom heating, and downwind building-wall heating) and various aspect ratios (0.5, 1, 1.5, 2, 2.5, 3, and 3.5).

It was shown that in the cases of upwind building-wall heating, one vortex appears regardless of aspect ratio. For aspect ratios greater than or equal to 1.5, the upward motion forced by upwind building-wall heating overcomes the mechanical downward motion that appears in the cases of no heating. In the cases of street-canyon bottom heating, for aspect ratios of less than 3, flow patterns are similar to those in the cases of upwind building-wall heating. This similarity results from the shift of the maximum temperature axis toward the upwind side caused by the horizontal motion. However, for aspect ratios of 3 and 3.5, the horizontal velocity is not strong enough to shift the maximum temperature axis toward the upwind side and therefore the maximum temperature axis is located near the center of the street canyon. In these cases, two counterrotating vortices appear side by side in the lower layer due to the thermally forced upward motion around the axis, while the vortex in the upper layer is little influenced by bottom heating. In the cases of downwind building-wall heating, two counterrotating vortices appear except for the case with an aspect ratio of 0.5. To a large extent, the vortex in the upper layer is mechanically induced by the ambient wind, while the vortex in the lower layer is thermally induced by downwind building-wall heating.

It was shown that the dispersion of pollutants released at the street level is quite dependent upon the aspect ratio and the location of the heat source. It also was shown that the vortex number and intensity in the street canyon greatly influence the residue concentration ratio by controlling the travel pathway and escape time of pollutants.

The current study clearly indicates that the building-wall or street-canyon bottom heating can significantly affect flow and dispersion in urban street canyons. In this study, we fixed the initial temperature difference between the air and the building wall or street-canyon bottom at 5 K. Since the temperature difference plays an important role in determining the number and inten-

sity of vortices in the urban street canyon and hence the dispersion characteristics, sensitivity experiments of the temperature difference are needed to understand better the phenomenon in the street canyon. In this study, we systematically examined thermal effects on the flow and pollutant dispersion when the building wall or street-canyon bottom is uniformly heated. However, in the real world, the building wall or street-canyon bottom is not uniformly heated by solar irradiation because the sky view factor changes depending upon the aspect ratio and solar zenith angle. For a more realistic simulation, it is desirable to include such physical factors in numerical models. We plan to implement the sky view factor into the numerical model to better understand flow and dispersion characteristics in the urban street canyon. Along with these modeling efforts, an extensive field study also is needed to better understand thermal effects on street-canyon flow and dispersion.

Acknowledgments. The authors are very grateful to anonymous reviewers for providing valuable comments on this study. This research was supported by Cray Research, Inc. through the 1998 University Research and Development Grant of the Systems Engineering Research Institute (SERI), Korea. The authors acknowledge SERI for providing a computing environment on the Cray C90 for this research.

REFERENCES

Abadie, P., and R. Schiestel, 1986: Prevision numérique de la convection forcée turbulente dans une cavité bidimensionnelle entrainée. *Int. J. Heat Mass Transfer,* **29,** 417–427.

Baik, J.-J., and J.-J. Kim, 1999: A numerical study of flow and pollutant dispersion characteristics in urban street canyons. *J. Appl. Meteor.,* in press.

Ciofalo, M., and M. W. Collins, 1989: $k-\varepsilon$ predictions of heat transfer in turbulent recirculating flows using an improved wall treatment. *Numer. Heat Transfer,* **15B,** 21–47.

DePaul, F. T., and C. M. Sheih, 1986: Measurements of wind velocities in a street canyon. *Atmos. Environ.,* **20,** 455–459.

Hoydysh, W. G., and W. F. Dabberdt, 1988: Kinematics and dispersion characteristics of flows in asymmetric street canyons. *Atmos. Environ.,* **22,** 2677–2689.

Hunter, L. J., I. D. Watson, and G. T. Johnson, 1990–91: Modelling air flow regimes in urban canyons. *Energy Build.,* **15–16,** 315–324.

——, G. T. Johnson, and I. D. Watson, 1992: An investigation of three-dimensional characteristics of flow regimes within the urban canyon. *Atmos. Environ.,* **26B,** 425–432.

Jayatilleke, C. L. V., 1969: The influence of Prandtl number and surface roughness on the resistance of the laminar sublayer to momentum and heat transfer. *Prog. Heat Mass Transfer,* **1,** 193–329.

Johnson, W. B., W. Dabberdt, F. Ludwig, and R. Allen, 1971: Field study for initial evaluation of an urban diffusion model for carbon monoxide. Contract CAPA-3-68 (1–69), SRI Project 8563, 69 pp. [Available from Stanford Research Institute, Menlo Park, CA 94025.]

Lanzani, G., and M. Tamponi, 1995: A microscale Lagrangian particle model for the dispersion of primary pollutants in a street canyon: sensitivity analysis and first validation trials. *Atmos. Environ.,* **29,** 3465–3474.

Lee, I. Y., and H. M. Park, 1994: Parameterization of the pollutant transport and dispersion in urban street canyons. *Atmos. Environ.,* **28,** 2343–2349.

Nakamura, Y., and T. R. Oke, 1988: Wind, temperature, and stability conditions in an east–west-oriented urban canyon. *Atmos. Environ.,* **22,** 2691–2700.

Nunez, M., and T. R. Oke, 1977: The energy balance of an urban canyon. *J. Appl. Meteor.,* **16,** 11–19.

Oke, T. R., 1988: Street design and urban canopy layer climate. *Energy Build.,* **11,** 103–113.

Patankar, S. V., 1980: *Numerical Heat Transfer and Fluid Flow.* McGraw-Hill, 197 pp.

Sakakibara, Y., 1996: A numerical study of the effect of urban geometry upon the surface energy budget. *Atmos. Environ.,* **30,** 487–496.

Sini, J.-F., S. Anquetin, and P. G. Mestayer, 1996: Pollutant dispersion and thermal effects in urban street canyons. *Atmos. Environ.,* **30,** 2659–2677.